

# EUVE Observations of clusters of galaxies: Virgo and M87

Thomas W. Berghöfer<sup>1,2</sup> and Stuart Bowyer<sup>1</sup> and Eric Korpela<sup>1</sup>

*Space Sciences Laboratory, University of California, Berkeley, CA 94720-7450, USA*

## ABSTRACT

We present results of a re-analysis of archival EUVE data of the central region of the Virgo cluster. We employ the new analysis method developed by Bowyer, Berghöfer & Korpela (1999) and find diffuse emission reaching out to a distance of  $\approx 13'$ . The spatial distribution of this flux is incompatible with a thermal plasma origin. We investigate whether this emission is due to inverse Compton scattering of relativistic electrons against the  $3^\circ$  K black-body background. We show that this emission cannot be produced by an extrapolation to lower energies of the observed synchrotron radio emitting electrons and an additional component of low energy relativistic electrons is required. In addition to discussing the diffuse EUV emission, we present an analysis of the EUV emission originating from the jet in M87.

## 1. Introduction

Observations with the *Extreme Ultraviolet Explorer* (EUVE) have provided evidence that a number of clusters of galaxies produce intense EUV emission (e.g., Bowyer et al. 1997). The initial explanation for this emission was that it is produced by a diffuse,  $(5-10) \times 10^5$  K thermal gas component of the intracluster medium (ICM). Gas at these temperatures cools very rapidly, however, and there is no obvious energy source to re-heat it (Fabian, 1996). Consequently, a number of other mechanisms have been investigated as the source of the emission. Inverse Compton (IC) scattering of cosmic microwave background photons by relativistic electrons present in the ICM was proposed as the source of the observed EUV emission in the Coma cluster (Hwang 1997; Enßlin & Biermann 1998). However, Bowyer & Berghöfer (1998) have shown that the spatial distribution of the EUV emission in this cluster is not consistent with IC emission from the observed population of relativistic electrons.

A variety of alternative explanations has been advanced which dismiss the EUVE excess in clusters of galaxies. Most recently, Arabadjis & Bregman (1999) argue that the EUV excess can be explained away by a different cross section for absorption by hydrogen and helium in the foreground ISM column. Bowyer, Berghöfer & Korpela (1999) find that in some clusters this may account for

---

<sup>2</sup>Hamburger Sternwarte, Universität Hamburg, Gojenbergsweg 112, D-21029 Hamburg, Germany

some of the excess present in the ROSAT PSPC data, however, this cannot explain the intense EUV excesses found with EUVE.

Bowyer, Berghöfer & Korpela (1999) reexamined EUVE data of the clusters Abell 1795, Abell 2199, and Coma. They demonstrated that the initially reported results are based on an improper background subtraction. In previous analyses a flat background had been assumed. However, a detailed investigation of blank field observations with the EUVE Deep Survey (DS) instrument shows that the background consists of two independent components, a non-photonic background and a background due to photons. The non-photonic background level can be determined in obscured regions of the detector and can be directly subtracted from the raw data. However, the photonic background is affected by telescope vignetting and must be treated differently.

In the case of Abell 1795 and Abell 2199, Bowyer, Berghöfer & Korpela (1999) show that the extent of the diffuse EUV emission is much smaller than earlier reported. Furthermore, the radial EUV emission profiles of these two clusters show a flux deficit compared to the soft energy tail of the X-ray emitting intracluster gas. These findings are consistent with the presence of strong cooling flows in Abell 1795 and Abell 2199.

In this paper we employ our new reduction method to EUVE archival data of the central part of the Virgo cluster. We compare our results with results derived from radio observations of this region. We consider the possibility that the observed diffuse EUV excess emission is due to an inverse Compton process of the known population of relativistic electrons in the ICM near M87. Furthermore, we investigate the emission originating from the jet in M87 and compare our results with observations at other wavelengths.

## 2. Data and Data Analysis

The Virgo cluster has been observed for 36,000 s with the Deep Survey (DS) Telescope of EUVE (Bowyer & Malina, 1991). Data reduction was carried out with the EUVE package built in IRAF which is especially designed to process EUVE data.

In order to reduce the non-photonic (non-astronomical) background contribution to the data we investigated the pulse-height spectrum of all detected events. A large number of EUVE DS observations of all kinds of astronomical targets has shown that a typical pulse-height spectrum consists of two components, a Gaussian profile representing the source events and an exponential background distribution. More details about the different background contributions to the DS data and the method of pulse-height thresholding can be found in Berghöfer et al. (1998). From our experience with stellar and extragalactic observations with EUVE we know that the pulse-height selection effectively reduces the non-astronomical background in the data without any significant reduction of the source signal. By comparing the source signal with and without pulse-height selection we find that the effect on the source signal is lower than 4%.

Then we applied corrections for detector dead time and for telemetry limitations (primbsching) to the screened event list and produced a DS EUV image of the Virgo cluster. We then determined the non-photonic background level in the image from highly obscured regions at the outer most parts of the field of view near the Lexan/B filter frame bars. This non-astronomical background contribution is assumed to be constant over the entire detector field and was subtracted from the image.

In order to subtract the (vignetted) photonic background we computed the azimuthally averaged radial emission profile centered on M87. We used the EUVE DS sensitivity map provided by Bowyer, Berghöfer & Korpela (1999) to determine a radial sensitivity profile centered on the detector position of M87. This was then fit to the outer part (15–20′) of the radial emission profile to determine the scaling factor between sensitivity profile and the photonic background in the data. The radial emission profile and the best fit background model are shown in Figure 1.

### 3. Results

The data in Figure 1 demonstrate the presence of diffuse EUV emission in the vicinity of M87 which extends to a radius of  $\approx 13'$ . At larger radii the radial profile is well fit by the background model demonstrating the absence of any significant cluster emission beyond this. The initial publication on the diffuse EUV emission from Virgo (Lieu et al. 1996) claimed to detect excess emission to 20′.

In Figure 2 we plot the background subtracted radial EUV emission profile (solid line). The dashed line shows the expected EUV emission of the low energy tail of the X-ray emitting diffuse intracluster gas as derived in the following. Note that the inner 1′ bin is dominated by the core and jet of M87 and must be ignored for the discussion of the diffuse emission.

To determine the diffuse X-ray contribution to the observed EUV emission we processed ROSAT PSPC archival data of the Virgo cluster. We used standard procedures implemented in the EXSAS software package to produce an image from the photon event list. Then a vignetting corrected exposure map was computed for this data set and a PSPC count rate image was generated by dividing the PSPC image by the exposure map.

We point out that the background in the ROSAT PSPC hard energy band is dominated by the photonic (vignetted) background and the contribution of the non-photonic background is minor. Therefore, a similar analysis as described for the EUVE DS data including a separation of the photonic and non-photonic background contributions is not essential. However, in the case of detectors with low effective areas (e.g., BeppoSAX), and less efficient rejection mechanisms for non-photonic events, this background contribution must be treated separately.

For our analysis of the ROSAT PSPC data we selected only photon events in the hardest energy band, channels 90–236. This channel selection has several advantages: First, any contamination by

a possible steep-spectrum source at soft X-ray energies is excluded and, therefore, ensures that this band pass represents only thermal contributions to the overall diffuse emission in Virgo. Second, this part of the ROSAT band pass is nearly unaffected by interstellar absorption. This minimizes errors due to possible differential ISM absorption effects when modeling conversion factors between DS and PSPC counts. Third, the count rate conversion factor between DS and PSPC is nearly temperature independent in the range of X-ray temperatures measured in the central Virgo region and, thus, ROSAT count rates of the diffuse X-ray emission can be converted into DS count rates by using one single conversion factor.

In order to be able to convert PSPC counts into DS counts we modeled conversion factors for a range of plasma temperatures (0.1–2.7 keV) employing the MEKAL plasma emission code with abundances of 0.34 solar (Hwang et al. 1997). These calculations include absorption by the interstellar medium. We used an ISM absorption column density of  $1.72 \times 10^{20} \text{cm}^{-2}$  (Hartmann & Burton 1997) and an absorption model including cross sections and ionization ratios for the ISM as described in Bowyer, Berghöfer & Korpela (1999). In Figure 3 we show the DS to PSPC count rate conversion factor. The left-hand scale and the solid curve gives the plasma temperature as a function of the DS to PSPC count rate ratio. As can be seen, for a wide range of temperatures (0.6–2.7 keV) the model conversion factor is constant within 15%. According to Böhringer et al. (1995) and Böhringer (1999), the temperature of the X-ray emitting intracluster gas in the Virgo cluster is  $\approx 2$  keV. In addition to this thermal gas component these authors detected several diffuse emission features near M87 which are significantly softer than the average Virgo cluster gas temperature. However, spectral fits to the ROSAT data do not provide any evidence for gas at temperatures below 1 keV (Böhringer, private communication). For temperatures near 1 keV the modeled conversion factor for a thermal gas is slightly lower than for higher temperatures. Therefore, the contribution of the lower temperature components to the overall diffuse X-ray emission in the EUV band pass is lower than the dominant 2 keV cluster gas component. Using the conversion factor appropriate for the mean cluster gas temperature of 2 keV for the entire emission including the softer thermal enhancements, slightly overestimates the low energy X-ray contribution to the EUV emission.

We also modeled the DS to PSPC conversion factor for a non-thermal power law type spectrum including ISM absorption. The right-hand scale and dashed curve give the power law spectral index as a function of the modeled conversion factor.

In Figure 4 we show the observed ratio between azimuthally averaged radial intensity profiles observed with the EUVE DS and PSPC. Within the error bars the ratio is constant (reduced  $\chi^2 = 0.9$ ). The best fit value is  $0.0186 \pm 0.0057$ . The ratio for the inner  $1'$  bin is consistent with this value, however, we excluded this point due to the presence of emission from the core and jet of M87. Sarazin & Lieu (1998) have suggested that an increasing EUV to X-ray emission ratio towards larger distances from the cluster center is an indication of an inverse Compton process producing the EUV emission in the cluster. However, the data in Figure 4 demonstrate that this is not observed in the central Virgo region.

Our best fit value of 0.0186 is  $\approx 4.3$  times larger than expected for the low energy tail of the X-ray emitting gas in the Virgo cluster. Therefore, the X-ray contribution to the observed EUV excess in the central part of the Virgo cluster must be minor.

It is clear that the ratio between observed EUV flux and modeled X-ray contribution cannot directly be used to determine the physical parameters of the source. Instead, one must first subtract the X-ray contribution from the observed EUV emission.

In Figure 5 we show the spatial distribution of the EUV excess emission in the central Virgo region; the background and the contribution of the low energy tail of the X-ray emitting ICM have been subtracted. The central emission peak at the position of M87 is surrounded by a diffuse EUV emission structure which is asymmetric in shape. Its extent varies between  $1'$  and  $7'$ . Several arm-like features are visible. At larger radii the EUV emission results from a number of apparently discrete and extended diffuse features in the M87 radio halo region. These emission features are consistent with the emission seen in the surface brightness profile (Figure 2) between  $9$ – $13'$ . These asymmetric features show the flux is not produced by a gravitationally bound thermal gas. For the diffuse EUV emission within  $7'$  (excluding the core + jet emission in the inner  $1'$ ) we determine a total count rate of  $(0.036 \pm 0.006)$  counts  $s^{-1}$ . Assuming an extraction radius of  $13'$  results in a total count rate of  $(0.066 \pm 0.009)$  counts  $s^{-1}$ .

We also investigated the EUV emission peak at the position of M87. X-ray observations with the *Einstein* and ROSAT HRIs have demonstrated that the central X-ray emission peak splits into two major components which are associated with the core and mainly knots A+B+C of the jet in M87. The spatial resolution of the EUVE DS ( $\approx 20''$ ) is not sufficient to completely resolve the jet from the galaxy core. However, the central peak indicates emission slightly elongated by about one resolution element in the direction from the core to the jet. The central emission peak (core + jet) provides a total count rate of  $(4.9 \pm 0.6) \times 10^{-3}$  counts  $s^{-1}$  in excess of the diffuse emission component.

## 4. Discussion and Conclusions

### 4.1. Diffuse EUV emission

The results of our reanalysis show a clear EUV excess in the central Virgo region around M87. Compared to previous studies the azimuthally averaged extent of this emission is smaller and extends only to  $\approx 13'$  from the center of M87.

To explore the nature of the EUV excess we compare this emission with a 90 cm radio map of the central Virgo region near M87 (Owen, Eilek & Kassim 1999). If the diffuse EUV emission is due to inverse Compton processes in the ICM, one would expect to see similar emission features in both the EUV and radio image. In Figure 6 we show a contour plot of the EUV emission superposed on the 90 cm radio map. As can be seen, the EUV emission peaks at the position of the radio emission

of the core and jet of M87. EUV excess emission features are, however, not directly coincident with any of the other brighter features visible in the radio map. The EUV emission is also not associated with the higher temperature X-ray emission features seen in the ROSAT PSPC images in Virgo (cf. Böhringer 1999 and Harris 1999).

We next investigate whether the integrated flux of the diffuse EUV emission is compatible with an inverse Compton origin of the observed EUV excess in the central Virgo region. We use the observed radio synchrotron power law spectrum of the M87 halo ( $\alpha = 0.84$ , Herbig & Readhead 1992) to compute the underlying distribution of relativistic electrons in this region and its inverse Compton flux. Note that the radio spectrum needs to be extrapolated into the low frequency range near 1 MHz which is not observable due to ionospheric effects. The conversion from the synchrotron spectrum into an electron energy distribution depends on the magnetic field strength in the ICM. We derive a relation between magnetic field strength and the inverse Compton flux produced by the relativistic electrons; the results are shown in Figure 7. The flux is folded with the EUVE DS response and given in units of DS counts  $s^{-1}$  which allows a direct comparison to the observed integrated DS count rate of the diffuse emission (horizontal line in Figure 7). As can be seen, for a magnetic field strength of  $\approx 3\mu\text{G}$  the observed flux matches the model flux. Note that this value would also be consistent with Faraday rotation measurements in the M87 halo (Dennison 1980).

However, with  $\alpha = 0.84$  the radio synchrotron spectrum is inconsistent with the required steep EUV to X-ray power law spectrum. In Figure 3 we show three dotted vertical lines labeled with 100%, 10%, and 5%. These lines indicate relative contributions of the hard energy tail of the EUV excess component to the overall X-ray emission in the ROSAT band. A contribution of 100% is obviously not realistic since this would require that no emission is seen from the gravitationally bound intracluster gas. The other two dotted lines show 10% and 5% contributions, respectively. No other emission component in excess of the thermal component has been detected in the ROSAT PSPC data of Virgo and only an upper limit can be derived from this data. A determination of an accurate upper limit for the EUV excess component in the ROSAT band is highly model dependent. However, from our experience with ROSAT data of diffuse sources we estimate that a contribution of 10% should be detectable. If we assume a 10% contribution as the upper limit for the EUV excess component in the ROSAT band, according to Figure 3 a power law photon number index of  $\alpha \geq 3.2$  is required to explain the observed EUV flux and the upper limit in the ROSAT PSPC hard band (channels 90–238) by a non-thermal power law source. Therefore, inverse Compton emission from the known population of relativistic electrons in the M87 halo cannot account for the observed EUV excess in the central Virgo region.

We compute the total luminosity of the diffuse EUV emission for a steep non-thermal power law spectrum and for a low temperature thermal plasma spectrum since these have been discussed in the literature, but we make no claim that either of these are the correct spectral distribution for the emission. Assuming a power law spectrum with  $\alpha = 3.2$  results in a luminosity of  $5.2 \times 10^{42}$  erg  $s^{-1}$  in the 0.05–0.2 keV band. For a thermal plasma with a temperature of 0.15 keV we obtain a luminosity of  $5.7 \times 10^{42}$  erg  $s^{-1}$ . These values were derived from the total count rate of the diffuse

EUV emission within  $7'$ . Including the apparently discrete and extended diffuse EUV emission detected between  $7'$  and  $13'$  increases the luminosity by 80%. Assuming larger power law indices or lower plasma temperatures result in higher luminosities. For the luminosity calculations we assume a distance of 17 Mpc.

#### 4.2. EUV emission of the jet in M87

Since the core and jet of M87 cannot be resolved in the EUVE image of M87, we assume that the X-ray flux ratio between core and jet which can be determined from the ROSAT HRI observations is also valid for the EUV fluxes. Harris, Biretta & Junor (1997) give a ratio of  $\approx 1.5$  for the core/jet X-ray flux ratio. Based on their compilation of measurements for the jet in M87, Meisenheimer et al. (1996) derived a spectral index of 0.65 for the radio to near-UV spectrum. In order to be able to explain the X-ray emission of the jet in M87 by the same spectrum, these authors introduced a spectral cut-off near  $10^{15}$  Hz. The spectral index of the UV to X-ray power law spectrum then has to be  $\alpha \approx 1.4$  to explain the UV and X-ray data.

Based on these assumptions we compute a flux of  $3.4 \times 10^{-12}$  erg cm $^{-2}$  s $^{-1}$  ( $6.5 \times 10^{-6}$  Jy) and a luminosity of  $1.2 \times 10^{41}$  erg s $^{-1}$  for the emission of the M87 jet in the EUVE DS bandpass. For the luminosity calculation we assume a distance of 17 Mpc.

In Figure 8 we show the radio-to-X-ray spectrum of the jet in M87 including the EUVE data point. As can be seen, the spectral model provided by Meisenheimer et al. (1996) also fits the EUVE observations. This confirms the suggested cut-off in the UV and further supports that the entire jet emission, from the radio to the X-ray band, is synchrotron radiation produced by relativistic electrons in the jet.

### 5. Summary

The observed EUV excess in the central Virgo region is not spatially coincident with either the distribution of the radio emission or the observed high temperature thermal X-ray emission seen in the ROSAT images. This provides strong evidence that a separate source mechanism is present. In addition, due to the required steep EUV to X-ray spectrum, this emission cannot be produced by an extrapolation to lower energies of the observed synchrotron radio emitting electrons. If the observed EUV excess is inverse Compton emission, a new population of relativistic electrons is required. Therefore, the same difficulties as in the case of the explanation of the EUV excess of the Coma cluster (cf. Bowyer & Berghöfer 1998) exist in the central Virgo region. The EUVE observations of M87 are consistent with the spectral cut-off in the spectrum of the jet in M87 as suggested by Meisenheimer et al. (1996). This further supports the idea that the EUV and X-ray emission of the jet is synchrotron radiation.

We thank Jean Eilek for providing us a postscript file of the M87 radio map. We acknowledge useful discussions with John Vallerga, Jean Dupuis, and Hans Böhringer. This work was supported in part by NASA contract NAS 5-30180. TWB was supported in part by a Feodor-Lynen Fellowship of the Alexander-von-Humboldt-Stiftung.

## REFERENCES

- Arabadjis, J. S. & Bregman J. N., 1999, *ApJ*, 514, 607
- Berghöfer, T. W., Bowyer, S., Lieu, R., & Knude, J. 1998, *ApJ*, 500, 838
- Böhringer, H., Nulsen, P. E. J., Braun, R. & Fabian, A. C. 1995, *MNRAS*, 274, L67
- Böhringer, H. 1999, Ringberg workshop
- Bowyer, S., & Malina, R. F. 1991, in *Extreme Ultraviolet Astronomy*, ed. R. F. Malina & S. Bowyer (New York: Pergamon), 397
- Bowyer, S., Lieu, R., & Mittaz, J. P. 1997, *IAU Symposium No. 188: The Hot Universe*, p. 52
- Bowyer, S., & Berghöfer, T. W. 1998, *ApJ*, 506, 502
- Bowyer, S., Berghöfer, T. W. & Korpela, E. 1999, *ApJ*, in press
- Dennison, B. 1980, *ApJ*, 236, 761
- Enßlin, T., & Biermann, P. 1998, *A&A*, 330, 96
- Fabian, A. C. 1996, *Science*, 271, 1244
- Harris, E. D., Biretta, J. A., & Junor, W. 1997, *MNRAS*, 284, L21
- Harris, E. D. 1999, Ringberg workshop
- Hartmann, D., & Burton, W. B. 1997, *Atlas of Galactic Neutral Hydrogen* (Cambridge: Cambridge Univ. Press)
- Herbig, T., & Readhead, A. C. S. 1992, *ApJS*, 81, 83
- Hwang, U., Mushotzky, R. F., Loewenstein, M., Markert,
- Hwang, C.-Y. 1997, *Science*, 278, 1917
- Lieu, R., Mittaz, J., Bowyer, S., et al. 1996, *ApJ*, 458, L5
- Meisenheimer, K., Röser, H.-J., Schlötelburg, M. 1996, *A&A*, 307, 61
- Owen, F., Eilek, J. & Kassim, N., 1999, in prep.



Sarazin, C., & Lieu, R. 1998, ApJ, 494, L177

Fig. 1.— The azimuthally averaged radial intensity profile of the EUV emission in the central part of Virgo (centered on M87) is shown as a solid line. The dashed line is the vignettted background. There is no EUV emission beyond  $\approx 13'$ .

Fig. 2.— The solid line shows the azimuthally averaged radial intensity profile of the background subtracted EUV emission in the central part of Virgo. The dashed line provides the contribution of the low energy tail of the X-ray emitting intracluster gas. The central  $1'$  bin is dominated by the core and jet in M87 and must be ignored in the context of diffuse emission.

Fig. 3.— Conversion factors from ROSAT PSPC count rates into EUVE DS rates modeled for a spectrum of a thermal plasma model and a non-thermal power law type source including the ISM absorption towards the Virgo cluster. Ordinates: Left-hand scale and solid curve give the plasma temperature for the thermal model; right-hand scale and dashed curve give the power law spectral index for the non-thermal model. Three dotted vertical lines labeled with 100%, 10%, and 5%. These lines indicate relative contributions of the hard energy tail of the EUV excess component to the overall X-ray emission in the analyzed ROSAT band (see Sect. 4.1).

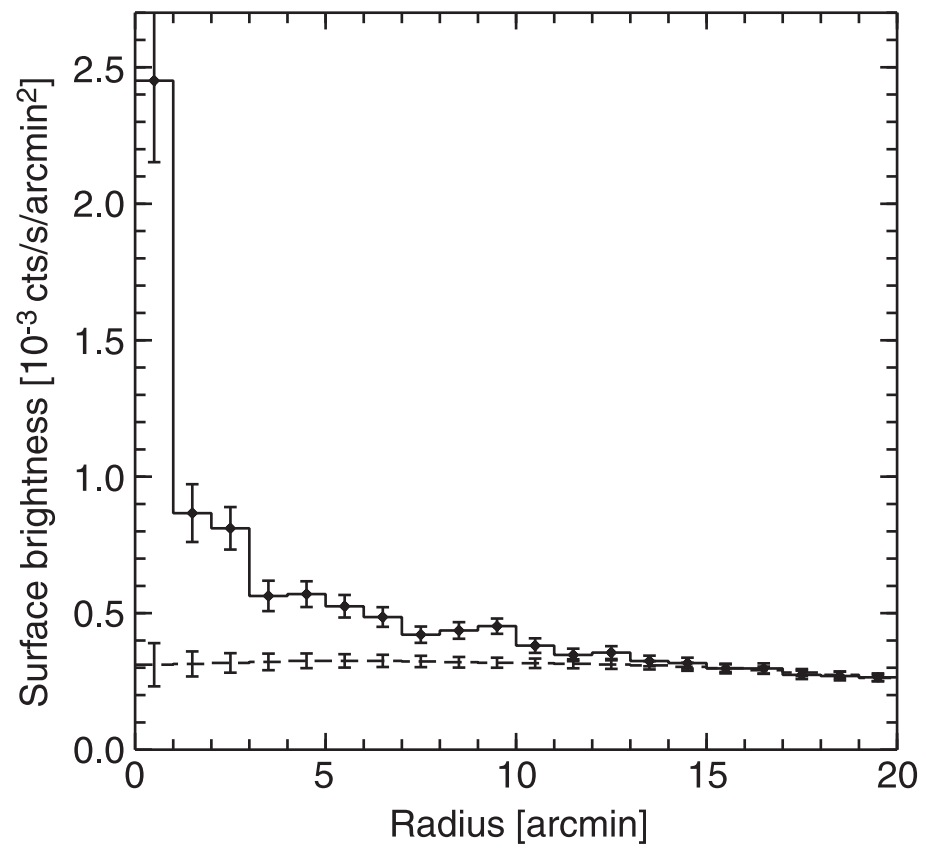
Fig. 4.— The ratio between observed azimuthally averaged intensity profiles observed with the EUVE DS and ROSAT PSPC. The dotted line represents the best fit value of 0.186 assuming a constant ratio.

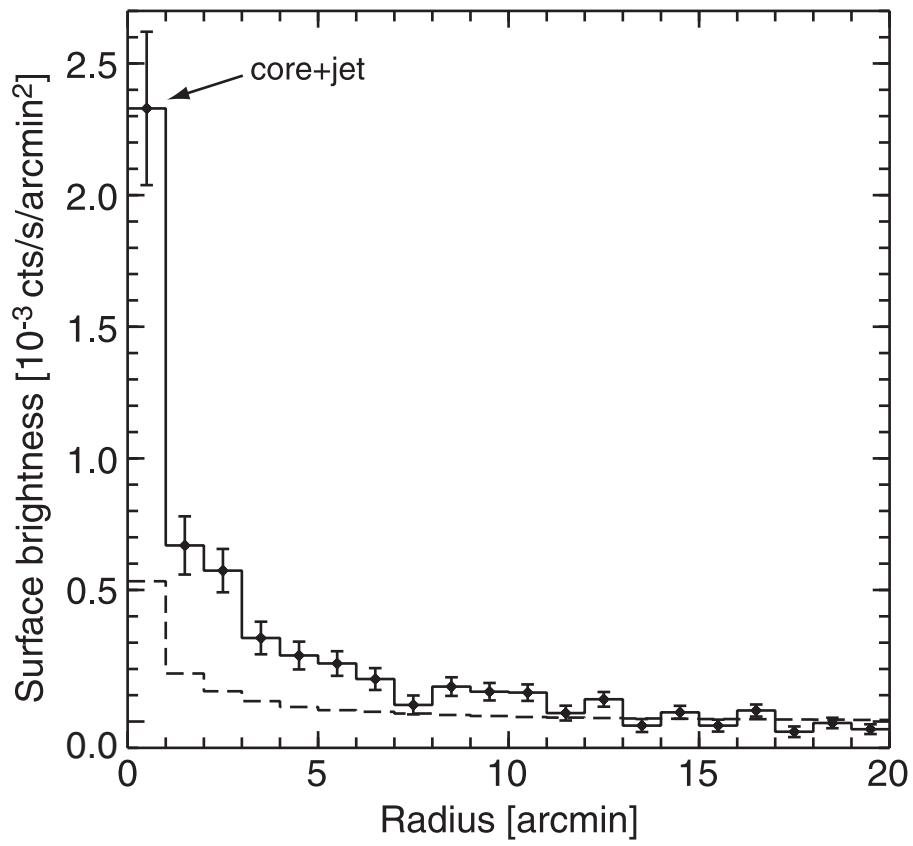
Fig. 5.— Spatial distribution of the EUV excess emission in the central Virgo region. The contribution of the low energy tail of the X-ray emitting ICM has been subtracted from the data.

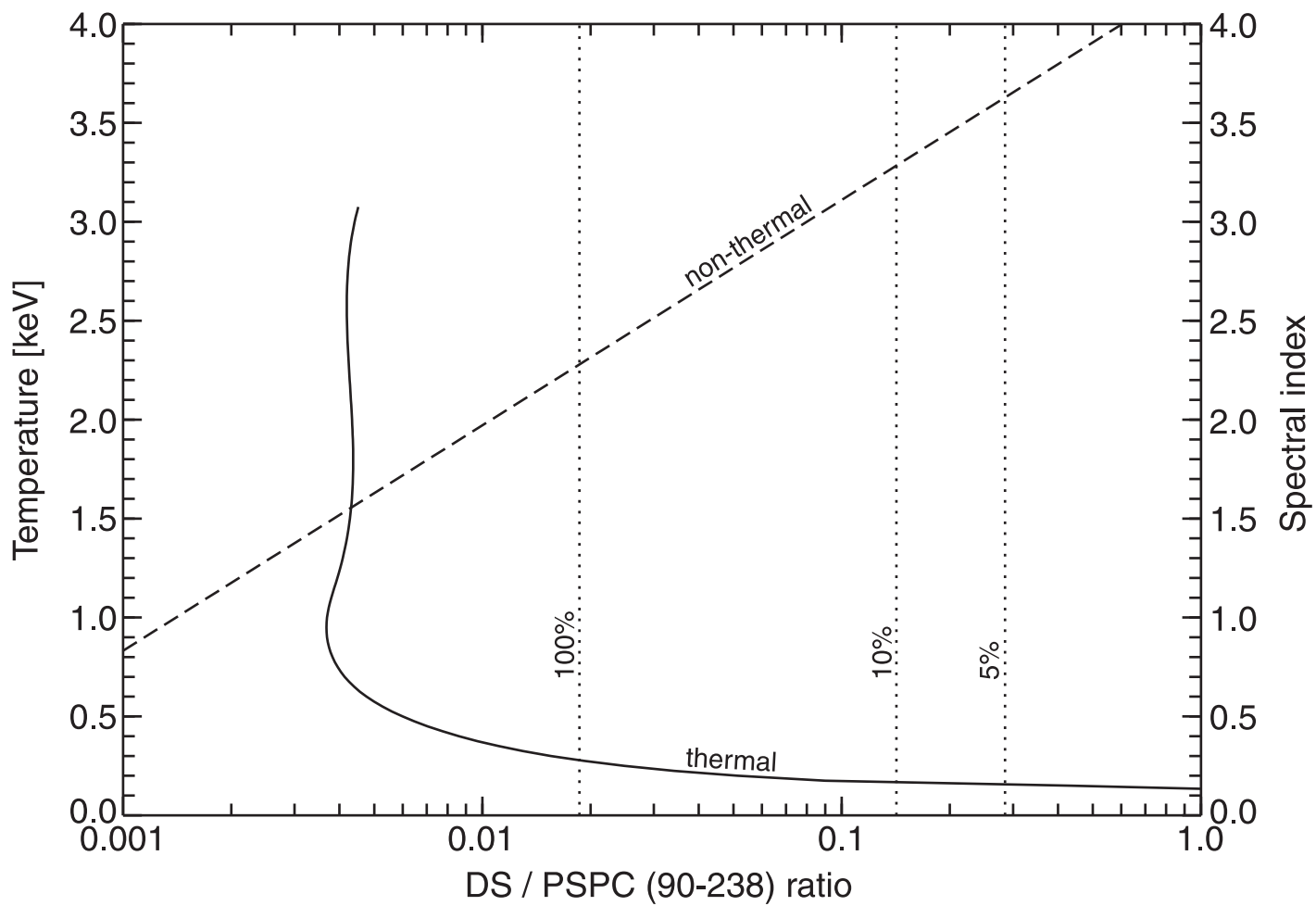
Fig. 6.— Contour plot of the background and X-ray subtracted EUV emission shown superposed on the 90 cm radio map of the M87 halo. The contours provide fluxes of 1.5, 4.5, 7, 10, 13, and 27  $\sigma$  above the noise level.

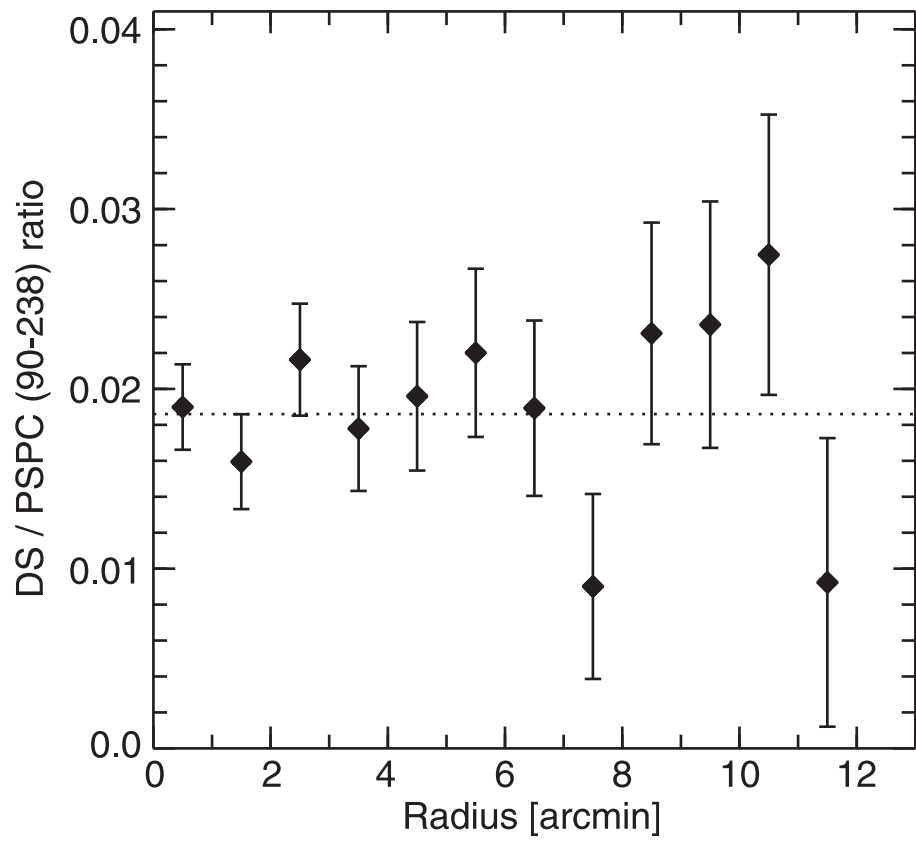
Fig. 7.— EUVE DS count rate as a function of magnetic field strength. The horizontal line provides the observed total count rate for the diffuse emission component. The error in this value is shown as a gray shaded area.

Fig. 8.— Radio-to-X-ray spectrum of the jet in M87 The solid line shows the model provided by Meisenheimer et al. (1996). The EUVE data point is well fit by this model with a cut-off at UV wavelengths.









This figure "figure5.jpg" is available in "jpg" format from:

<http://arxiv.org/ps/astro-ph/9912421v1>

This figure "figure6.jpg" is available in "jpg" format from:

<http://arxiv.org/ps/astro-ph/9912421v1>

